

The *Gaia* *GSP-Spec* catalogue of interstellar extinctions, and stellar luminosities, radii, and masses

Patrick de Laverny¹, Alejandra Recio-Blanco¹, Camila Navarrete¹, Pedro A. Palicio¹, and Emanuele Spitoni²

¹ Université Côte d’Azur, Observatoire de la Côte d’Azur, CNRS, Laboratoire Lagrange, Bd de l’Observatoire, CS 34229, 06304 Nice cedex 4, France

² I.N.A.F., Osservatorio Astronomico di Trieste, via G.B. Tiepolo 11, 34143, Trieste, Italy

Received ??, 2026 ; accepted ??

ABSTRACT

The *Gaia*/DR3 *GSP-Spec* module has published the atmospheric parameters of up to 5.6 million stars based on the analysis of their Radial Velocity Spectrometer spectra. By combining these spectroscopic parameters with *Gaia* parallax and photometric measurements, a large catalogue of interstellar colour excesses and extinctions, complemented with stellar luminosities, radii, and masses, was constructed without relying on any stellar evolution or structure models. This catalogue also contains the associated uncertainties estimated from Monte-Carlo realisations for about 4.6 million stars. We present a system of quality flags based on the *GSP-Spec* quality parameters, the achieved numerical precision, and the *Gaia* astrometric quality. Adopting these flags, we defined a subsample of high-accuracy and precision parameters of more than 1.5 million stars. The impact of possible *GSP-Spec* parameter inaccuracies on the derived extinctions, luminosities, radii, and masses was also explored and revealed that the mass is the most affected quantity. The radii and masses were validated by comparison with interferometric and asteroseismic data. This confirmed their high quality, even when the targets were highly extinguished by the interstellar medium. We also emphasise that they are fully compatible and homogeneous with the *GSP-Spec* parameters. This allowed us to avoid systematics and biases that might be hidden when data from different (and potentially) heterogeneous catalogues are combined. Finally, we present some example applications of this catalogue: (i) exoplanet radii and masses, (ii) present-day mass distribution functions, (iii) identification of Galactic populations based on their mass distribution, and (iv) Galactic halo accreted stellar luminosities and masses that confirm their merger epochs.

Key words. Stars: fundamental parameters, radius, mass. Interstellar reddening. Method: spectroscopy. Galaxy: stellar content

1. Introduction

Stellar parameters are essential for many fields in astrophysics, from exoplanetary, stellar, and Galactic to extragalactic studies. In general, the main stellar atmospheric parameters (effective temperature T_{eff} , surface gravity $\log(g)$, and mean metallicity $[M/H]$), plus the individual chemical abundances are estimated from the analysis of the light received from stars with photometric and/or spectroscopic methods. However, other fundamental stellar parameters cannot be directly derived from observations. This is generally the case, in particular, for the stellar radii (R) and masses (M), not to mention ages. Atmospheric parameters and chemical abundances depend on our knowledge of the physics of the studied stellar object. However, other fundamental parameters additionally depend on our capacity to predict how these physics evolve with time. For example, these quantities are often derived by adopting specific model-dependent techniques, such as isochrone fitting for the mass and ages (see, for instance, Taniguchi et al. 2026). These projection techniques are most often (and better) applied to main-sequence turn-off or sub-giant stars because their atmospheric parameters strongly depend on time for these specific evolutionary stages. Another successful method for deriving these stellar fundamental parameters is asteroseismology based on space observations, which can provide much better accuracies, but for only a few thousand red giants (Schonhut-Stasik et al. 2024; Pinsonneault et al. 2025, among others). The analysis of the stellar oscillations can indeed provide an accurate radius and mass, through seismic scal-

ing relations and knowing T_{eff} (see, for instance, Miglio et al. 2013). However, these asteroseismic data are not available for large samples of stars at any stage of their evolution, and in particular, for the main-sequence stars (Serenelli et al. 2017). For accurate stellar radius measurements, we might also cite interferometric techniques, which can provide good results, but for a rather small number of close stars with well-known distances (Salsi et al. 2020).

All of these methods depend on the knowledge of the stellar atmospheric parameters, in particular, T_{eff} and $[M/H]$. In this context, the ESA *Gaia* mission has revolutionised the availability of these stellar parameters by providing accurate and precise parallaxes for several hundred million stars (see, for the third data release, Gaia Collaboration et al. 2023b). For a small fraction of them, whose spectra was collected by the on-board Radial Velocity Spectrometer (RVS, Cropper et al. 2018), the *Gaia* *GSP-Spec* module derived the main stellar atmospheric parameters (T_{eff} , $\log(g)$, $[M/H]$ a proxy of $[Fe/H]$ ¹, and the α -element abundance enhancement with respect to iron $[\alpha/Fe]$) for up to 5.6 million stars (see Recio-Blanco et al. 2023, for an extensive description of *GSP-Spec*).

We here directly estimate supplementary fundamental parameters from the *GSP-Spec* parameters and adopt a different method than those described above without relying on any stellar evolution model. The interstellar colour excesses and extinc-

¹ The *GSP-Spec* metallicity parameter $[M/H]$ indeed traces the $[Fe/H]$ abundance ratio (see, Recio-Blanco et al. 2023, for details).

tions towards each *GSP-Spec* stars are indeed computed from their main atmospheric parameters and predicted colours. Then, after computing the bolometric corrections and adopting complementary *Gaia* astrometric and photometric data, we estimate the stellar luminosities. Finally, it is straightforward to derive the stellar radii and masses when T_{eff} and $\log(g)$ are known. All these parameters are thus fully consistent among each other and are free of any assumption of stellar evolution and/or structure. Our work is structured as follows. We first describe in Sect. 2 the computation of the interstellar colour excesses and extinction towards each *GSP-Spec* star and derive the stellar luminosities, radii, and masses in Sect. 3. Our catalogue content is presented in Sect. 4. We explore the effect of possible inaccuracies in the *GSP-Spec* atmospheric parameters on the interstellar absorption, stellar luminosity, radius, and mass computations in Sect. 5. The catalogue is then validated by a comparison with literature values in Sect. 6, and some application examples are discussed in Sect. 7. Our conclusions are finally summarised in Sect. 8.

2. Interstellar absorption

To compute stellar luminosities and other related quantities (see Sect. 3), the interstellar extinction in the *Gaia* band (A_G) towards each *GSP-Spec* target has to be estimated. For this purpose, we first computed new colour excesses and then extinctions by adopting a method that is fully consistent with the stellar parameters derived by *GSP-Spec*, considering only additional information from *Gaia* two-band photometry. Our extinctions can therefore be considered to be purely spectroscopic and have the advantage of not being affected by possible (T_{eff} , colour excess) degeneracies, unlike certain photometric methods.

2.1. Interstellar colour excess

Since dust reddens stellar colours, the comparison of intrinsic colours computed from the stellar atmospheric parameters with observed ones allows us to estimate the colour excess caused by the interstellar medium. This method assumes that the stars are accurately and precisely parametrised, which is the case for a very large subsample of the *GSP-Spec* stars. Practically, this exercise was performed for the *Gaia* B_P and R_P magnitudes, which are available for the whole sample. The colour excess (or reddening) in the *Gaia* bands is thus simply expressed by

$$E_{(B_P-R_P)} = (B_P - R_P)_{\text{Observed}} - (B_P - R_P)_{\text{Intrinsic}}. \quad (1)$$

The star colours without absorption, $(B_P - R_P)_{\text{Intrinsic}}$, were derived with Eq. 1 of Casagrande et al. (2021, C21 hereafter, see Eq. 2). This equation (called F_{C21} hereafter) allowed us to estimate the stellar T_{eff} based on a polynomial that depends on the observed intrinsic colour, $\log(g)$ and $[M/H]$. We recall that a very good agreement in the low-extinction regime between the *GSP-Spec* parameters and the C21 relation was already confirmed by Recio-Blanco et al. (2023, see their Fig. 19). This is expected because the two studies relied on similar Solar abundances and stellar atmospheric models, although they were fully independent.

Based on this equation F_{C21} and adopting the *Gaia* $(B_P - R_P)$ colour, the polynomial coefficients provided in the first line of Tab. 2 of C21, and considering their dwarf and giant separation as a function of the stellar colour, we solved the equation

$$T_{\text{eff}} - F_{C21}[(B_P - R_P)_{\text{Intrinsic}}, \log(g), [M/H]] = 0, \quad (2)$$

in which we adopted the *GSP-Spec* T_{eff} , $\log(g)$ and $[M/H]$ values. However, this relation does not take the possible effect on

the metallicity of the stellar chemical content into account. We therefore considered in Eq. 2 a mean metallicity corrected for the stellar $[\alpha/\text{Fe}]$ content, adopting the relation proposed by Salaris et al. (1993). For the *GSP-Spec* stars without published $[\alpha/\text{Fe}]$ (11% of the full catalogue), we assumed that their α content follows the classical Galactic disc relation with metallicity, $[\alpha/\text{Fe}] = 0.0$ dex for $[M/H] \geq 0.0$ dex, $[\alpha/\text{Fe}] = +0.4$ dex for $[M/H] \leq -1.0$ dex and $[\alpha/\text{Fe}] = -0.4 \times [M/H]$ for $-1.0 \leq [M/H] \leq 0.0$ dex. These $[\alpha/\text{Fe}]$ -corrected metallicities were adopted throughout for estimating the other parameters, when necessary.

Furthermore, we recall that the adopted atmospheric parameters were deliberately published uncalibrated by *GSP-Spec*, and we favoured the recommended calibrations here as a function of T_{eff} , as indicated hereafter. For the surface gravity and metallicity, we adopted the calibrations provided in Appendix A of Recio-Blanco et al. (2024), and for $[\alpha/\text{Fe}]$, we adopted the calibration provided in Table 4 of Recio-Blanco et al. (2023) as a function of T_{eff} . The surface gravity calibration was then slightly improved to further increase the accuracy of $\log(g)$. For this purpose, a final second-order calibration considering gravity and metallicity effects was applied, based on a comparison with APOGEE/DR17 data (Abdurro'uf et al. 2022). We refer to de Laverny et al. (2025) for details on this supplementary calibration. We note that the adopted relations hereafter are weakly dependent on the surface gravity (except the stellar mass determination). The values we computed are thus almost unaffected by possible small calibration inaccuracies. We finally recall that the recommended calibrations have published validity ranges. For parameters found outside these ranges, we did not extrapolate the calibration polynomials and simply adopted the limit correction values corresponding to the range boundaries.

Eq. 2 is easily solved numerically by adopting $(B_P - R_P)_{\text{Observed}}$ as a first guess, and then by iterating until a solution is reached at a 10^{-5} level. Typically, the colour excesses are quickly found in a few steps. Practically, $E_{(B_P-R_P)}$ were estimated by solving Eq. 2 1000 consecutive times. We adopted random values for T_{eff} , $\log(g)$, $[M/H]$, $[\alpha/\text{Fe}]$, and $(B_P - R_P)_{\text{Observed}}$ within their error bars and assumed a normal distribution for these uncertainties². These Monte-Carlo realisations led to rather Gaussian distributions of $E_{(B_P-R_P)}$. The colour excess values we report (see Sect. 4) are simply the median of the computed distributions. Their associated uncertainties are then half of the difference between the 84th and 16th quantiles of the distributions, and hence, they correspond to a 1σ uncertainty for a normal distribution.

2.2. Interstellar extinction

From the previously derived interstellar reddening, we computed the extinction in the *Gaia* band (A_G). For this purpose, we estimated the coefficients that relate this extinction and the colour excess for every star,

$$k_{TGMA} = A_G / E_{(B_P - R_P)}, \quad (3)$$

based on the tables provided with the *Gaia* stellar parameters³ (Creevey et al. 2023). These k_{TGMA} coefficients depend on the four atmospheric parameters derived by *GSP-Spec*: T_{eff} , $\log(g)$, $[M/H]$, and $[\alpha/\text{Fe}]$. As above, we also considered their associated uncertainties (including those of $E_{(B_P-R_P)}$) to compute 1,000

² We remind that the *GSP-Spec* parameter uncertainties mostly reflect the spectra S/N ratios.

³ <https://www.cosmos.esa.int/web/gaia/dr3-astrophysical-parameter-inference>

Monte-Carlo realisations that finally provided the median value of the A_G distributions and their uncertainties.

3. Stellar luminosities, radii, and masses

From the previously estimated interstellar extinction, we computed the stellar luminosity (L), radius (R), and then, the mass (M) for each *GSP-Spec* star. It is important to note that the above quantities are independent of any stellar evolutionary models and Galactic priors (except for the adopted distances; see below). We first computed the absolute stellar magnitude,

$$M_G = G_{\text{mag}} - 5 \times \log_{10}(d) + 5 - A_G, \quad (4)$$

where G_{mag} and d (in pc) are the DR3 magnitudes in the *Gaia* band and the Bailer-Jones et al. (2021) *geometric*⁴ stellar distances based on *Gaia*/DR3 parallaxes, respectively. The absolute bolometric magnitude is then

$$M_{\text{bol}} = M_G + BC_G, \quad (5)$$

where BC_G is the bolometric correction in the G filter, computed according to Casagrande & Vandenberg (2018). This depends on T_{eff} , $\log(g)$, and the α -corrected metallicity. The stellar luminosity expressed in Solar units is then easily obtained,

$$\log_{10}(L/L_{\odot}) = -0.4 \times (M_{\text{bol}} - M_{\text{bol}}^{\odot}), \quad (6)$$

where $M_{\text{bol}}^{\odot}=4.74$ is the adopted value for the absolute bolometric magnitude of the Sun (IAU 2015 resolution B2, Prša et al. 2016). The *GSP-Spec* effective temperature then allowed us to estimate the stellar radius with the Stefan-Boltzmann relation (Stefan 1879; Boltzmann 1884),

$$R/R_{\odot} = \sqrt{L/L_{\odot}} \times (T_{\text{eff}}^{\odot}/T_{\text{eff}})^2, \quad (7)$$

where R is expressed in Solar units, and the effective Solar temperature is fixed at $T_{\text{eff}}^{\odot}=5,777$ K. The stellar mass in Solar units was subsequently obtained using the surface gravity,

$$M/M_{\odot} = (R/R_{\odot})^2 \times (g/g_{\odot}), \quad (8)$$

where $\log(g_{\odot})=4.44$ with g in cm^2/s . We point out that precise stellar masses can only be derived from extremely precise g measurements, whereas spectral analysis methods provide $\log(g)$ estimates with typical uncertainties of about 0.1-0.2 dex. Again, we considered the uncertainties associated with all these quantities by performing 1,000 Monte-Carlo realisations, propagating the uncertainties on each atmospheric parameter. As above, we publish the median of the parameter distributions, and the associated uncertainties were estimated based on the 84th and 16th quantiles.

4. The *GSP-Spec* catalogue of interstellar absorption and stellar L , R , and M

The computed colour excesses, extinctions, luminosities, radii, and masses together with their associated uncertainties are reported in an electronic table (see Table 1 for its content) for each *GSP-Spec* star, when available. We also include in the table the calibrated atmospheric parameter values that were adopted in this paper.

⁴ These geometric distances were adopted to be consistent with Gaia Collaboration et al. (2023a).

Table 1. Content of the *Gaia GSP-Spec* catalogue of interstellar reddening, extinctions, stellar luminosities, radii, and masses.

Label	Description
GDR3Id	<i>Gaia</i> DR3 Identification
T_{eff}	Adopted effective temperature (K)
$T_{\text{eff_err}}$	T_{eff} uncertainty (K)
$\log(g)$	Adopted surface gravity (g in cm/s^2)
$\log(g)_{\text{err}}$	$\log(g)$ uncertainty
[M/H]	Adopted metallicity (dex)
[M/H]_{\text{err}}	[M/H] uncertainty (dex)
$[\alpha/\text{Fe}]$	Adopted enhancement in α -elts w.r.t. Fe (dex)
$[\alpha/\text{Fe}]_{\text{err}}$	$[\alpha/\text{Fe}]$ uncertainty (dex)
E_BpRp	Colour excess in (B_p-R_p) (mag.)
E_BpRp_err	$E_{(B_p-R_p)}$ uncertainty (mag.)
A_G	Extinction in the G -band (mag.)
A_G_err	A_G uncertainty (mag.)
L	Stellar luminosity (in L_{\odot})
L_err	L uncertainty (in L_{\odot})
R	Stellar radius (in R_{\odot})
R_err	R uncertainty (in R_{\odot})
M	Stellar mass (in M_{\odot})
M_err	M uncertainty (in M_{\odot})
Flag_Param	QF associated to the <i>GSP-Spec</i> parameters (0/1/2) = (High/Good/Moderate)-Quality
Flag_Ext	QF associated to the extinction calculation (0/1/2) = (High/Good/Moderate)-Quality
Flag_LRM	QF associated to the L , R , and M derivation (0/1/2) = (Very high/High/Medium)-Quality (9) = Low-Quality astrometric parameters and/or <i>LRM</i> filtered out (see text)

Notes. The full version of this table is available at CDS.

4.1. Parameter accuracy and quality flags

Together with these parameters, we also publish three quality flags (QF , best value=0) that allow one to select the best derived quantities. Except for the first flag, the two additional quality flags are specific to the derivation of the new parameters derived here. These new QFs are defined as described below:

- The goal of $Flag_{\text{Param}}$ is to summarise the flag chain of *GSP-Spec* into a single value for the use of the new data presented here. We recall that the 13 first *GSP-Spec* QFs refer to the quality of the T_{eff} , $\log(g)$, and [M/H] estimates (see for more details Sect.8 of Recio-Blanco et al. 2023), mostly depending on the quality of the input RVS spectra. The best parametrised (~ 1.9 million stars, i.e. $\sim 40\%$ of the ~ 4.6 million included in this catalogue) for which all their first 13 *GSP-Spec* flags are equal to 0 therefore have $Flag_{\text{Param}}=0$. Moreover, $Flag_{\text{Param}}=1$ (2) refers to stars for which at least one of these 13 first QFs is equal to 1 (2), and this affects $\sim 35\%$ stars of the whole sample (2; 25% stars). We note that about 20% of all the *GSP-Spec* stars were rejected from our catalogue because the quality of their parameters was too low, as revealed by one of their *GSP-Spec* QFs being equal to 9 (some of them being also KM-giant flagged stars, see Recio-Blanco et al. 2023).
- $Flag_{\text{Ext}}$ allows one to select targets with the best interstellar absorption estimates. It should therefore be considered when dealing with $E_{(B_p-R_p)}$ and/or A_G , but also with L , R , or M because these quantities rely directly on the interstellar extinction estimate. It can take values of 0, 1, or 2 (from

high quality to moderate quality, respectively) and was determined by considering the accuracy reached when numerically solving Eq. 2. Stars whose $(B_P - R_P)_{\text{Observed}}$ colour was found to be outside the validity range of the F_{C21} function in Eq. 2 were filtered out. Typically, this occurred for stars that are too cool. The very few stars for which Eq. 2 cannot be numerically solved were also filtered out. We proceeded similarly for stars whose effective temperature was outside the recommended range by C21 (i.e. cooler than 3600 K or hotter than 8500 K) and for those whose $\log(g)$ and/or $[M/H]$ was extrapolated with respect to the ranges of the synthetic spectrum reference grid adopted by *GSP-Spec*. In summary, as a consequence of these rejection criteria (including those related to $Flag_{\text{Param}}$), the total number of stars in the catalogue is ~ 4.6 million.

- $Flag_{\text{LRM}}$ assesses the quality of the L , R , and M computation. Basically, this flag was estimated by propagating the $Flag_{\text{Ext}}$ value and considering whether the $\log(g)$ and $[M/H]$ values adopted for the computation of the bolometric correction are well found within the validity ranges recommended by Casagrande & Vandenberg (2018). Four different values are provided: 0, 1, and 2 for very high, high, and medium-quality determinations; and determination with a quality that is too low are identified by $Flag_{\text{LRM}}=9$. Moreover, no LRM values are published for the $\sim 1.4\%$ stars with $Flag_{\text{LRM}}=9$, and when Eq. 2 cannot be solved and/or when no BC_G were estimated because their stellar atmospheric parameters are found to lie outside the validity ranges provided by Casagrande & Vandenberg (2018). In contrast, some stars with $Flag_{\text{LRM}}=9$ have published $LRMs$. They have possible *Gaia* astrometric issues that might affect their distance (and thus, L) estimates. These stars either have a *Gaia* astrometric *ruwe* parameter larger than 1.4 or a *fidelity* factor lower than 0.5, following Rybizki et al. (2022); both of these indicate a poor astrometric solution. Possible non-single stars are also found in this category and were identified by considering the *Gaia* keywords *duplicated_source* and *non_single_star*. In total, all these astrometric criteria affect about 20% of all the *GSP-Spec* stars. We finally note that some variable stars might be included in our catalogue. Future users should check their parameters since the *GSP-Spec* analysis might have been affected by the stacked-epoch RVS spectra.

Moreover, a final check was specifically performed for the derived masses since it is well known that for some stars, the surface gravity might be difficult to derive accurately from their spectra. Because M varies linearly with g (and not with $\log(g)$, as indicated in Eq. 8), rather large uncertainties in $\log(g)$ lead to huge M uncertainties. For instance, a 0.3 dex in $\log(g)$ uncertainty corresponds to a relative mass error larger than a factor of 2 (i.e. $\sim 100\%$ for M). This should be considered when building working samples for specific scientific applications (see below). Furthermore, we also searched for possible large inconsistencies between the *GSP-Spec* $\log(g)$ and a luminosity-based surface gravity estimate, as was done in de Laverny et al. (2024). These were simply estimated by computing $\log(g)_{\text{Lum}} = \log(g_{\odot}) + \log(M) - \log(L) + 4 \times \log(T_{\text{eff}}^{\odot})$, adopting a very wide range of possible masses. About 10^4 stars with likely poor *GSP-Spec* gravities were then identified when the difference between the spectroscopic and luminosity-based surface gravities was larger than 2 dex. Their masses were rejected from the catalogue, but the other derived parameters remained included because they depend very weakly on $\log(g)$.

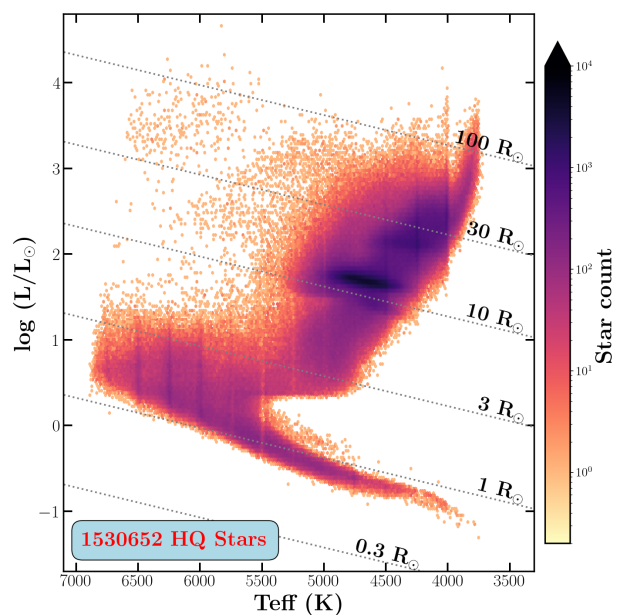


Fig. 1. Stellar luminosity vs. effective temperature diagram for the high-quality subsample (see text for its definition), colour-coded by the stellar count. The dotted lines represent the iso-radius relations.

Finally, in addition to these quality flags, we also recommend to consider the reported uncertainties associated with the different parameters in order to define high-quality subsamples that are especially adapted for specific applications. For instance, stellar radii and masses for stars with a large luminosity uncertainty (e.g. $\geq 30\%$) should be considered with caution. Moreover, the mass of stars with a surface gravity uncertainty larger than ~ 0.3 dex could be filtered out. We also encourage future users to also adopt the quality flag system of Recio-Blanco et al. (2023) to more precisely select stars with optimal T_{eff} , $\log(g)$ and $[M/H]$ derivations instead of considering $Flag_{\text{Param}}$. The spectra S/N and the *GSP-Spec* χ^2 quality-fit parameter could also be considered.

4.2. Catalogue content and typical uncertainties

In the catalogue presented in Table 1, we finally publish the colour excess and extinction for 4.6 million stars, that is, 82% of the whole *GSP-Spec* catalogue. Luminosity and radius are provided for 99.7% of them, and the mass is provided for 99.5%. In this catalogue, 62% of the stars have their three $QF \leq 1$, meaning a good-quality derivation, and 1.52 million stars (33%) have very high quality parameters with $Flag_{\text{Param}}=Flag_{\text{Redd}}=Flag_{\text{LRM}}=0$. As an illustration of the catalogue content, we show in Fig. 1⁵ and 2 diagrams of the luminosity versus effective temperature for a high-quality (*HQ*) subsample, colour-coded by stellar count, the extinction, and the stellar mass. These 1.53 million *HQ* stars (about one-third of the total sample) were selected by applying the following criteria: $(Flag_{\text{Param}}=0) \& (Flag_{\text{Redd}} \leq 1) \& (Flag_{\text{LRM}} \leq 1)$, plus a relative error on the luminosity lower than 30%. Only for exploring the stellar masses, we then restricted this *HQ* sample to stars

⁵ In this figure, the overdensity features seen at some T_{eff} reference grid points are caused by overfitting patterns produced by the *GSP-Spec* algorithm in the high- S/N regime (see Recio-Blanco et al. 2023, for more details).

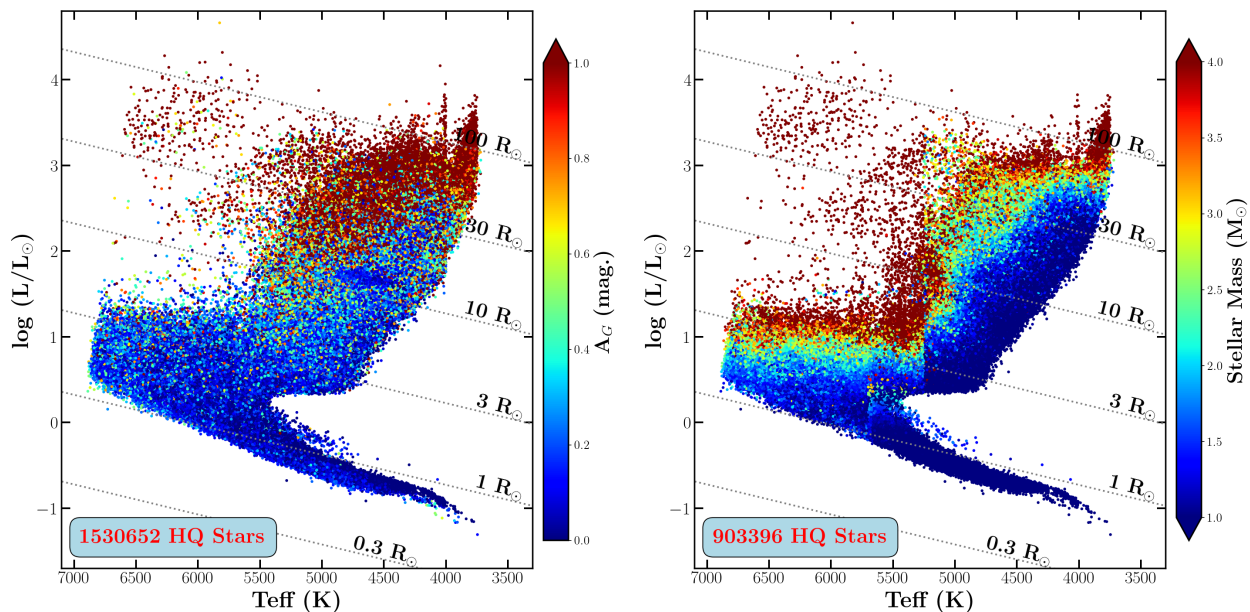


Fig. 2. Same as Fig.1, but colour-coded by interstellar absorption and stellar mass (from left to right).

with $\log(g)_{\text{err}} < 0.1$ (i.e. equivalent to an error on g lower than 25%), leading to about 900,000 stars with a rather well-defined mass (20% of the total sample). The mean uncertainties associated with this *HQ* sample are equal to 0.02 and 0.03 mag for $E_{(B_p-R_p)}$ and A_G , and 6%, 3%, and 22% for the mean relative uncertainties on L , M , and R , respectively. The largest relative errors on R and M are equal to 16 and 40%. This *HQ* sample is also characterised by (i) $\sim 24,000$ stars with a luminosity lower than $0.5 L_\odot$ and $\sim 22,000$ high-luminosity stars ($L > 500 L_\odot$), (ii) $\sim 20,000$ dwarfs with a radius smaller than $0.8 R_\odot$ and ~ 500 giants defined by $R > 100 R_\odot$ (only two have $R > 200 R_\odot$), and (iii) $\sim 9,000$ stars are less massive than $0.6 M_\odot$ and $\sim 2,300$ are more massive than $10 M_\odot$ (168 with $M > 50 M_\odot$). More exotic stars should be explored outside the *HQ* sample by relaxing the quality flags. This Fig. 1 shows that the different evolutionary stages of stars of any masses are well represented. The majority of the most reddened stars are the most luminous, massive, and hence, distant stars belonging to the Galactic halo, whereas a few other massive stars are much closer but deeply embedded in the thin disc. In contrast, the main sequence is highly dominated by low-mass dwarfs with low extinction since they are not very distant. Finally, at any stage, a correlation between L and M is clearly seen.

5. Effect of the atmospheric parameter accuracy on the derived A_G , L , R , and M

The uncertainties on A_G , L , R , and M provided in Table 1 were directly estimated from the uncertainties of the atmospheric parameters (T_{eff} , $\log(g)$, $[M/H]$, and $[\alpha/Fe]$) reported in the *GSP-Spec* analysis. We recall that these uncertainties result from the RVS spectrum noise and are thus only related to the precision of the parameter derivation. We next explore the effect of the accuracy of the atmospheric parameter derivation on the new quantities we derived.

For this purpose, we simply (i) considered some test stars typical of the lower main sequence, the turn-off, the lower Red Giant Branch (RGB), the clump of the Horizontal Branch, and the Asymptotic Giant Branch (AGB; see Table 2 for their param-

eter values), (ii) varied their atmospheric parameter as if they were inaccurate, (iii) rederived their A_G , L , R , and M , and finally quantified the effect of these inaccuracies. For each test star, we adopted Solar metallicity and $[\alpha/Fe]$, and we considered no uncertainties on the distance and magnitudes. The inaccuracies we explored for T_{eff} , $\log(g)$, $[M/H]$, and $[\alpha/Fe]$ were 100 K, 0.25 dex, 0.1 dex, and 0.1 dex, respectively. These values are typical of those associated with spectroscopic surveys.

First, as shown in Table 2, possible inaccuracies in $[M/H]$ and $[\alpha/Fe]$ do not affect any of our parameters at all, regardless of the stellar type, because these two atmospheric parameters only act in Eq. 2 and 3 and on the bolometric correction, and the dependence of these relations on these parameters is rather weak for an inaccuracy of 0.1 dex. Similarly, and for the same reasons, the inaccuracy in $\log(g)$ does not affect the derivation of A_G , and L and R are safely estimated (with an uncertainty of $\sim 1\%$) regardless of the stellar type. In contrast, an inaccurate T_{eff} by 100 K can lead to rather strong variation in the absorption of 0.05 up to 0.2 mag, and thus, to luminosity variations of typically $\sim 5\text{--}10\%$. The stellar mass and radius are less affected by ΔT_{eff} , however, with a possible variation of up to $\sim 3\%$. This effect is stronger for the giant stars. It is simply caused by a significant change in the theoretical stellar colour when T_{eff} is varied (derived from Eq. 2), which then affects Eq. 1, and, as shown in Eq. 7 and 8, ΔR and ΔM vary mostly as $\Delta T_{\text{eff}}/T_{\text{eff}}^{-3}$. Finally, and as expected when examining Eq. 8, the mass of all star types is strongly modified by about $\sim 75\%$ for an inaccuracy in $\log(g)$ of only 0.25 dex.

In summary, interstellar extinction and stellar luminosities are accurately derived for stars with quite accurate effective temperatures. Similarly, we also recommend adoption of the masses published here for stars with very accurate stellar gravities. We excluded masses from our *HQ* sample derived from $\log(g)$ with uncertainties larger than 0.1 dex for this reason (among others; see the previous section). We also refer to Sect. 6.3 and the validations with asteroseismic masses, which confirm this behaviour.

⁶ In Table 2, we provide only the effect on A_G since it is identical as the one on $E_{(B_p-R_p)}$.

Table 2. Effect of possible atmospheric parameter inaccuracies on the quantities derived here.

		Main Sequence (5000 K, 4.5)	Turn-Off (6500 K, 3.5)	Lower RGB (4800 K, 3.0)	Clump (4500 K, 2.5)	AGB (4000 K, 1.5)
$\Delta T_{\text{eff}}=100$ K	$\Delta (A_G)$	0.07 mag	0.05 mag	0.09 mag	0.11 mag	0.18 mag
	$\Delta(L, R, M)$	(5.1, 1.5, 2.9)%	(4.8, 0.7, 1.6)%	(5.9, 1.1, 2.3)%	(6.8, 1.1, 2.3)%	(11., 0.2, 0.3)%
$\Delta \log(g)=0.25$ dex	$\Delta (A_G)$	0.01 mag	0.02 mag	0.02 mag	0.01 mag	0.01 mag
	$\Delta(L, R, M)$	(0.8, 0.4, 77.)%	(1.1, 0.6, 75)%	(1.5, 0.7, 75.)%	(0.8, 0.4, 77.)%	(1.1, 0.5, 76)%
$\Delta[M/H]=0.1$ dex	$\Delta (A_G)$	0.01 mag	0.01 mag	0.01 mag	0.01 mag	0.01 mag
	$\Delta(L, R, M)$	(1.1, 0.6, 1.2)%	(0.7, 0.3, 0.9)%	(0.7, 0.3, 0.7)%	(0.6, 0.3, 0.6)%	(0.8, 0.4, 0.8)%
$\Delta[\alpha/Fe]=0.1$ dex	$\Delta (A_G)$	0.01 mag	0.01 mag	0.01 mag	0.01 mag	0.01 mag
	$\Delta(L, R, M)$	(0.7, 0.4, 0.6)%	(0.4, 0.2, 0.6)%	(0.4, 0.2, 0.5)%	(0.5, 0.3, 0.3)%	(0.6, 0.3, 0.9)%

Notes. These test stars are typical of different evolutionary stages. Their adopted effective temperatures and surface gravities are provided in the second line. Solar $[M/H]$ and $[\alpha/Fe]$ are adopted for all of them.

6. Validation with the literature

In this section, the *Gaia* *GSP-Spec* catalogue of interstellar reddening and stellar radii and masses is compared to literature values for validation purposes. We first summarise some of our previous comparisons of $E_{(B_p-R_p)}$, R , and M with published values, and we then focus on more global validations of our stellar radii through interferometric angular diameters and of our R and M exploiting asteroseismic data. We note that we did not consider stellar radii derived from surface brightness-colour relations for these validations because they require specific calibrations that might be affected by distance and reddening uncertainties, in contrast to asteroseismic determinations (see, for instance, the series of articles from Valle et al. 2024).

6.1. Previously published comparisons

6.1.1. Interstellar reddening

The computed colour excesses towards each *GSP-Spec* star have been extensively discussed and compared to literature values by Barbillion et al. (2025). We refer to this paper for a detailed validation of the derived 2D and 3D *GSP-Spec* extinction maps. In brief, a very good agreement with the literature was found, and an excellent spatial correlation with already known interstellar medium structures such as molecular clouds and spiral arms was retrieved. This study therefore confirms the high quality of the interstellar reddening values in the present catalogue.

6.1.2. Radii and masses of specific stars

To validate the stellar radii and masses we estimated, we first referred to Recio-Blanco et al. (2024); de Laverny et al. (2025); Navarrete et al. (2025) who validated these quantities for specific stellar types, but for a rather small number of stars. More global comparisons performed for larger numbers of stars are presented in Sect. 6.2. First, Recio-Blanco et al. (2024) considered a sample of *GSP-Spec* stars with extremely precise atmospheric parameters. They found that our spectroscopic masses and those derived from combined Kepler and APOGEE data agree very well (APOKASC2, Pinsonneault et al. 2018) for stars with similar $\log(g)$ values in the two catalogues. These authors found a small bias of about $0.03 M_{\odot}$, associated with

a dispersion of $0.22 M_{\odot}$ (see their Fig. 4). Then, de Laverny et al. (2025, see their Appendix A) explored the stellar radii and masses for the exoplanet host stars in our catalogue and compared them with values derived from asteroseismic and spectroscopic data. Again, the agreement with the literature was found to be very good, with no bias and a dispersion of 4% for R and a bias of 4% associated with a dispersion of 17% for M . Finally, we also refer to Navarrete et al. (2025), who validated our masses for extreme cases (red giant binaries) and also found a satisfactory agreement with published values.

6.2. Global validation

In the following, we proceed with a more global validation of our whole catalogue, for which we not only consider some specific applications as described above. In order to facilitate the comparison, we only considered homogeneous reference catalogues of stellar radius and mass determinations, based on direct technics (i.e. the least model dependent), such as interferometry and asteroseismology.

6.2.1. Interferometric angular diameters

Our stellar radii can be directly compared to interferometric observations that provide stellar angular diameters, which, combined with the Bailer-Jones et al. (2021) distances we adopted, allow us to obtain a completely independent measurement of the stellar radius. For this comparison, we considered angular diameters of dwarfs and giants from the catalogue of Salsi et al. (2020, S20 hereafter), who implemented a selection of reliable interferometric measurements from the JMMC Measured Stellar Diameters Catalog (Duvert 2016). This catalogue contains 127 stars with a high-quality diameter measurement (adopting their `Rej_Keep` flag), 66 of which are also found in our catalogue. Fig. 3 shows a comparison between these interferometric stellar radii and our spectroscopic ones. An impressive agreement is found: the mean relative difference (computed as $(R_{GSP-Spec} - R_{S20})/R_{S20}$) is equal to 1% with a dispersion of only 3%. Moreover, this bias becomes null when we only consider the 44 stars belonging to our *HQ* sample, and the dispersion is

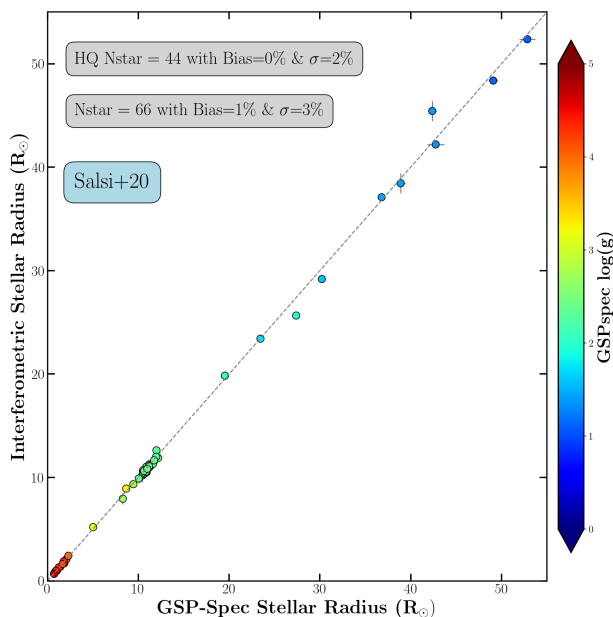


Fig. 3. Comparison between the measured interferometric stellar radii from Salsi et al. (2020) and our values. The 1:1 relation is shown as a dashed line. Most error bars are too small to be visible. The colour-coding represents the *GSP-Spec* surface gravity, which confirms the dwarf or giant nature of the S20 stars. When our 44 *HQ* stars are considered alone, the bias becomes null and the dispersion improves slightly.

reduced to 2%. The agreement between these two completely independent radius determinations is therefore excellent and validates the method we adopted, that is, not only the radius determination, but also the different previous steps described in Sect. 2 & 3: the derivation of the interstellar extinction, the bolometric correction, and the luminosity from the *GSP-Spec* parameters.

6.2.2. Asteroseismic radii and masses

We compared our best derived stellar radii and masses (*HQ* subsample) to completely independent estimates based on asteroseismic observations. For this purpose, we considered the radii and masses of giant stars derived by the APOKASC-3 and APO-K2 studies (Pinsonneault et al. 2025; Schonhut-Stasik et al. 2024, respectively) and the APOKASC values of Serenelli et al. (2017) for dwarfs and subgiants. The APOKASC and APO-K2 studies relied on Kepler (Borucki et al. 2008) and K2 datasets, respectively, which differ in several aspects: asteroseismic data analysis, target selection, shorter K2 observations, and so on. So, differences in radius and mass are expected between these studies (see an illustration below). Moreover, we recall that the asteroseismic radius depends on $T_{\text{eff}}^{1/2}$ and that our spectroscopic radius is estimated from the square root of the luminosity and T_{eff}^2 (see Eq.7). Similarly, the asteroseismic mass is related to $T_{\text{eff}}^{3/2}$ and the spectroscopic mass to $\log(g)$ (Eq. 8). In the following validations, we therefore restricted the comparison samples to stars with a difference in T_{eff} and $\log(g)$ smaller than 100 K and 0.1 dex, respectively, between the *GSP-Spec* and asteroseismic⁷ catalogues.

⁷ When available, we adopted their asteroseismic $\log(g)$ and not their spectroscopic values

APOKASC: The third version of the APOKASC catalogue (APOKASC-3) provides precise mass and radius estimates for about 10,000 red giants (i.e. corresponding to about two-thirds of their initial sample). These quantities were estimated based on Kepler asteroseismic measurements, *Gaia*/DR3 astrometric data (Gaia Collaboration et al. 2023b), and APOGEE/DR17 spectroscopic parameters (Abdurro'uf et al. 2022). In the following, we only considered their best-quality parameters, which belong to their Gold Category. Of their Gold stars, 4,533 are found in our *HQ* subsample, and 2,019 of them satisfy the adopted differences of 100 K and 0.1 dex in T_{eff} and $\log(g)$. Their radius and mass are compared in Fig. 4 (top panels). The stellar radii agree very well with a mean relative difference (bias) of only 2% and an associated standard deviation of 4%, in the sense of (*GSP-Spec* - literature)/literature. For the mass comparison, the agreement is also very satisfactory with a mean relative difference of 4% and a standard deviation of 15%. Moreover, most of the mass dispersion is clearly produced by the largest $\log(g)$ differences. When we only consider the 750 stars with $\Delta\log(g) < 0.05$ dex, the dispersion in mass is reduced to 10%.

For the dwarfs and subgiants, 176 of our *HQ* stars are also found in the Serenelli et al. (2017) catalogue of 415 stars. We recall that this catalogue is based on *Kepler* asteroseismic and APOGEE/DR13 spectroscopic data. Because of the lower statistics, we did not apply any filter on T_{eff} for the radius comparison, which is again found to be excellent, with a mean relative difference of 2% and a standard deviation of 4% (see Fig. 4, middle panels). For the mass comparison, we selected the 66 stars with an agreement in $\log(g)$ better than 0.1 dex. The bias (7%) and standard deviation (15%) are slightly larger than before, but this is explained by the differences in the adopted atmospheric parameters. The stars that depart most strongly from the 1:1 relation are those with the largest differences in T_{eff} and/or $\log(g)$. The larger error bars might also explain part of the dispersion. In any case, this comparison again confirms the high quality of the radius and mass spectroscopy determinations when compared to the APOKASC values.

APO-K2: This catalogue contains data for about 7,500 RGB and Red Clump stars, adopting K2-GAP DR3 asteroseismic data (Zinn et al. 2022), and, as APOKASC-3, *Gaia*/DR3 astrometric and APOGEE/DR17 spectroscopic data. About 2,500 of these giant stars are found in our catalogue, and 1,254 belong to our *HQ* subsample. The comparison of the two samples is shown in the bottom panels of Fig. 4, and we also applied the same filtering as for APOKASC-3 on ΔT_{eff} and $\Delta\log(g)$ (565 stars were left). As for the other comparison samples, the radii agree very well (bias and dispersion are equal to 2% and 8%, respectively). The slightly larger dispersion is simply explained by the larger number of stars that differ in T_{eff} by more than 50-100 K. The larger error bars are also associated with the seismic radii of the largest stars. The mass comparison is also affected by the rather large $\log(g)$ differences and rather large uncertainties in both samples, although the agreement is still satisfactory (bias of 5%).

6.3. Summary of the validations

The above comparisons confirm the high quality of our catalogue values, which rely on the spectroscopic *GSP-Spec* parameters. By selecting homogeneous, large, and high-quality reference catalogues of stellar radii and masses based on completely independent and direct techniques (i.e. the least model dependent) such as interferometry and asteroseismology, we found ex-

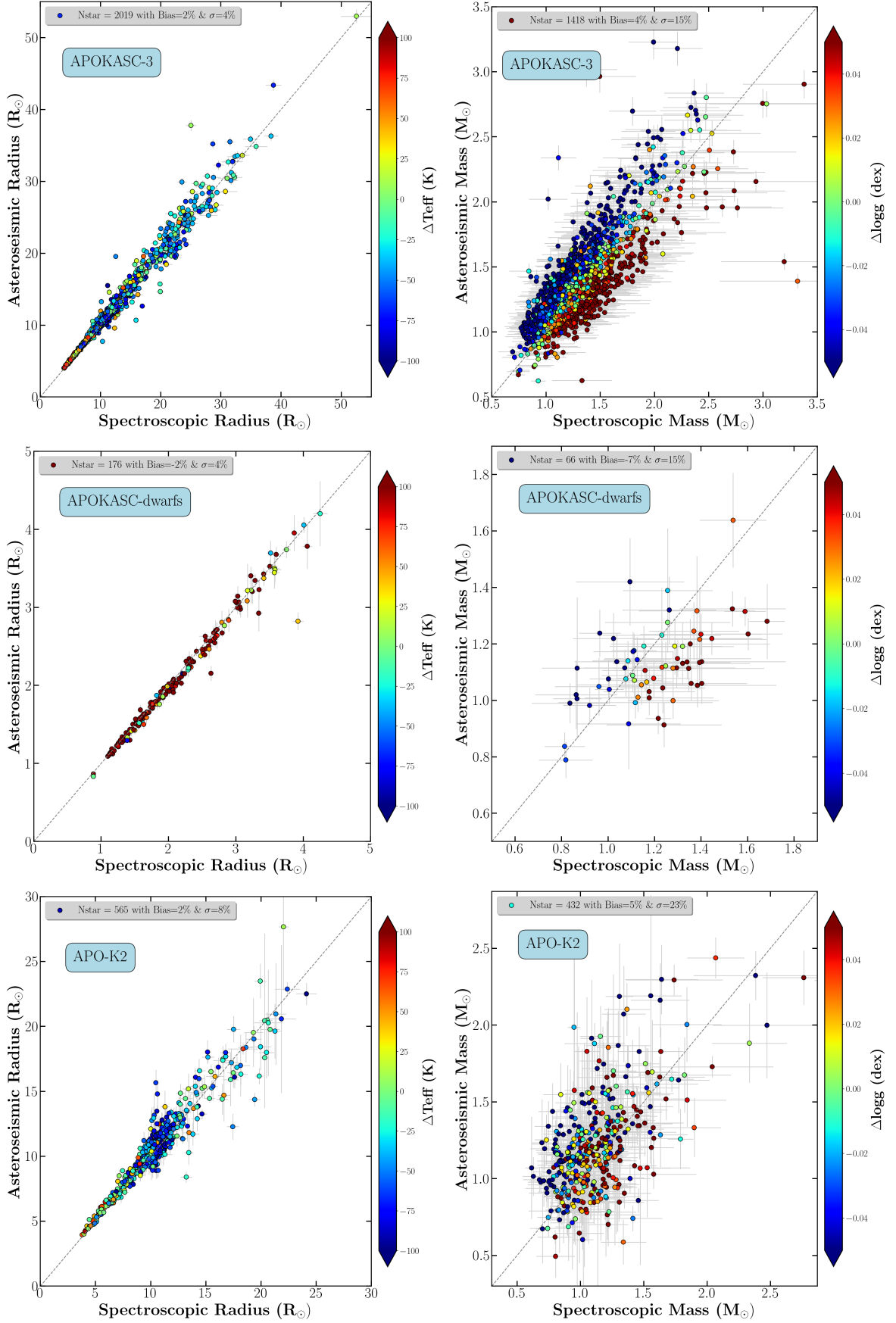


Fig. 4. Comparison between the *GSP-Spec* spectroscopic stellar radii (left panels) and masses (right panels) and those derived based on asteroseismic data by Pinsonneault et al. (2025); Serenelli et al. (2017); Zinn et al. (2022), shown in the top, middle, and bottom panels, respectively. The 1:1 relation is shown as a dashed grey line. The colour-codes represent the difference in T_{eff} and $\log(g)$ between the different samples in the sense (*GSP-Spec* - literature), left and right panels, respectively. The mean relative differences and associated standard deviations indicated in each panel are in the sense of (*GSP-Spec* - literature)/literature (see the associated text for more details).

cellent agreement with the literature. In particular, this agreement improved when we considered our high-quality subsample and when the effective temperatures and surface gravities adopted by the different works agreed, leading to even smaller dispersions. We emphasise that the agreement for the radii with respect to interferometric and asteroseismic data is particularly impressive (almost no biases, and dispersions of a few percent). This validates the whole method we adopted, that is, not only the radius determination, but also the derivation of the interstellar reddening, the bolometric corrections, and the luminosities from the *GSP-Spec* parameters, based on which we estimated R and M . For the mass comparison with asteroseismic data, typical relative differences are about 5% with dispersions of 15-20%. These numbers are improved by a factor of ~ 2 when we consider the smaller differences in the adopted T_{eff} and $\log(g)$, and this confirms the global very good agreement for such a difficult parameter derived directly from the spectroscopic data. Moreover, this section again supports what we showed in Sect. 5, that is, the stellar mass is most sensitive to the uncertainty in $\log(g)$. Therefore, this atmospheric parameter has not only a significant effect on M , but is also the main driver of its uncertainty. Finally, we also point out that some of the comparison sources used in this section have rather high extinctions (e.g. about 10% of our selected APOKASC-3 stars have $A_G > 0.2$, and ~ 50 of them have $A_G > 0.5$). This further reinforces our validation, because even with extinction, accurate stellar radii and masses are recovered.

7. Example applications of the catalogue

In order to illustrate the wide range of possible applications of our catalogue, we focus this section on different studies starting from exoplanet topics to Galactic ones. We recall that 2D and 3D interstellar dust maps based on our catalogue have been presented by Barbillon et al. (2025).

7.1. Radii and masses of exoplanets

A first example of an application of the *GSP-Spec* catalogue of stellar radii and masses was presented by de Laverny et al. (2025), who published a large, homogeneous, and precise catalogue of radii and masses of 3,556 exoplanets hosted by 2,573 stars. These new planet parameters were derived by rescaling the previously published planet parameter values, adopting the stellar radii and masses we estimated here. The lower uncertainty of the planet radii compared to literature values allowed these authors to improve the characterisation of the decrease in the number of small planets around $1.8 R_{\text{Earth}}$ (evaporation valley, Fulton et al. 2017). Among other results, a dichotomy between dense and inflated planets was also found. Denser planets defined by $R_p \leq 1.1 R_{\text{Jup}}$ appeared to be more massive for more metal-rich host stars. Conversely, inflated planets orbiting more metal-poor stars were found to be more massive. It was proposed that this bimodality might reveal that the diversity of giant exoplanets might depend on their Galactic birth locus. Dense giant planets were indeed found to be more numerous than inflated ones for supra-Solar metallicities, as in the central Milky Way regions. We refer to de Laverny et al. (2025) and forthcoming articles investigating the host star chemical properties for more details on the *Gaia* spectroscopic catalogue of exoplanets.

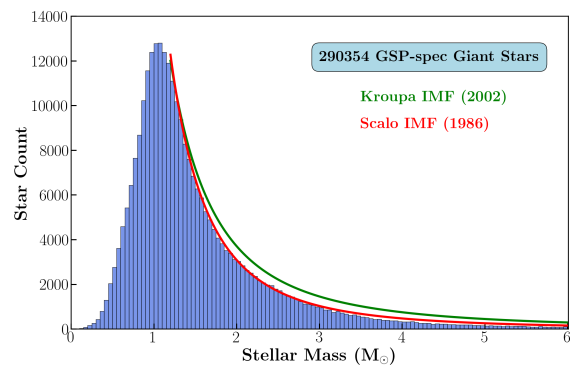


Fig. 5. Present-day mass function of a subsample of bright giant stars (see text for details about the adopted filtering selection) compared to the IMF of Scalo and Kroupa, whose power-law indexes are equal to 2.7 and 2.3, respectively.

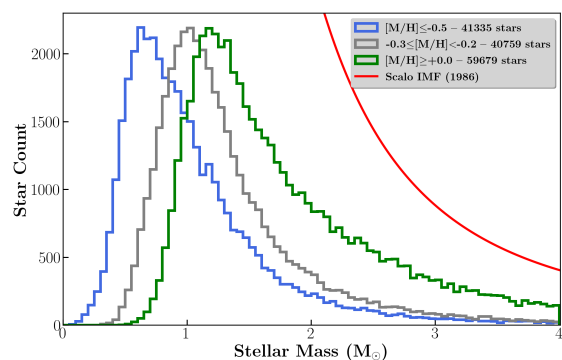


Fig. 6. Same as Fig. 5, but for the three metallicity bins indicated in the legend. The total number of stars in each histogram is also reported. The Scalo IMF is that of Fig. 5.

7.2. Stellar mass distributions

In order to explore the stellar mass distribution of our catalogue, which indeed corresponds to the Present-Day Mass Function (PDMF) and to compare it to theoretical Initial Mass Function (IMF), we first defined the most complete subsample, that is, a subsample not affected by observational biases. We focused on giant stars to do this because the *GSP-Spec* catalogue is known to be less complete for dwarfs. Then, following Fig. 2 of Recio-Blanco et al. (2023), the rise in *GSP-Spec* stellar counts with the G -magnitude clearly decelerates for stars fainter than ~ 12.5 . We therefore show in Fig. 5 the mass distribution of a subsample of almost 300,000 giant stars found in our catalogue, characterised by $L > 200 L_{\odot}$ and $G < 12$. Adopting the HQ subsample for our application biases the subsample by favouring high- S/N spectra and leading to a rougher distribution with a number of stars more massive than $\sim 2.5 M_{\odot}$ that is too large (and unrealistic). This figure shows that the PDMF of our giant stars agrees well with the IMF of Scalo (1986) over the range $\sim 1.2 - \sim 3.5 M_{\odot}$. Conversely, the Kroupa (2002) IMF⁸ predicts a number of stars more massive than $\sim 1.5 M_{\odot}$ that is too large and is not confirmed by our catalogue. We recall that the Scalo IMF was derived from Galactic field star counts and is therefore a composite IMF of many star-forming regions. It is thus expected that it fits our data well based on stellar counts in the Solar vicinity.

⁸ The IMF power-law indexes of the Salpeter and Kroupa distributions are too close (2.35 and 2.3) to be distinguishable in this figure.

Table 3. Median masses and Galactic orbital properties.

Metallicity range (units)	Mass (M_{\odot})	$\sigma(V_Z)$ (km/s)	Eccentricity
$[M/H] \geq 0.0$ dex	1.7	22.0	0.13 ± 0.09
$-0.3 \leq [M/H] < -0.2$ dex	1.2	27.1	0.15 ± 0.10
$[M/H] \leq -0.5$ dex	0.9	58.4	0.32 ± 0.25

Notes. The Galactic orbital properties correspond to the dispersion of the vertical velocity and the mean eccentricity plus its dispersion. The considered stars are the giants belonging to the three metallicity bins shown in Fig. 6.

This rather good agreement between our PDMF and the Scalo IMF can be understood by examining Fig. 6, which shows the PDMF for the same sample of giant stars, but only those belonging to three specific metallicity ranges. These ranges were defined in order to have rather similar number of stars and to span the metal-poor to the metal-rich regime. A rather smooth variation can be seen with a larger number of massive stars with increasing metallicity, but these PDMFs differ from the Scalo IMF, regardless of the normalisation factor. In particular, this figure shows that most stars with supra-Solar metallicities are more massive than the Sun, with several stars having $M > 2 M_{\odot}$. In contrast, almost all the most metal-poor stars ($[M/H] < -0.5$ dex) have masses lower than $1.5 M_{\odot}$, and their mass distribution is closest to the Scalo IMF. All of this is quantified in the first column of Tab. 3, which reports the median mass of these three metallicity ranges. The median absolute deviations associated with these medians are similar for the three ranges and equal to $\sim 0.5 M_{\odot}$. This increased number of massive stars for higher metallicities can easily be interpreted when we consider that the *GSP-Spec* sampled volume spans different Galactic populations. We indeed report in Tab. 3 some Galactic orbital parameters for the three metallicity bins that were computed by Palić et al. (2023). In particular, $\sigma(V_Z)$, the Galactic vertical velocity dispersion can be viewed as an age proxy of the stellar populations. This quantity indeed increases with time (see, for instance, Hayden et al. 2018, and references therein) because of the progressive dynamical heating of the disc. $\sigma(V_Z)$ is larger for the most metal-poor regime composed by lower-mass and thus, older, stars whose orbits have been heated. In contrast, the orbits of the most metal-rich and massive stars, which are younger, did not have time to be significantly perturbed (lower $\sigma(V_Z)$). All of this is fully consistent with the increasing eccentricities of the Galactic orbits (mean and dispersion, reported in the third column of Tab. 3) with decreasing metallicity.

We therefore conclude that the agreement between the PDMF and IMF shown in Fig. 5 is caused by an age effect. The most metal-poor massive stars have already ended their life and are thus absent from the blue histogram of Fig. 6, whereas the lower-mass stars in the same metallicity bin had enough time to evolve as giants. Conversely, most of the low-mass metal-rich stars are still on the main-sequence and are therefore not included in the green histogram. As a consequence, based on the mass distributions alone, we can claim that the most metal-rich bin of Fig. 6 is dominated by young stars that mostly belong to the Galactic thin disc, whereas the most metal-poor bin contains older stars of the Galactic thick disc or halo.

7.3. Galactic halo accreted stars

It is now widely admitted that the Galactic halo is in part composed of several substructures (some of them are called streams)

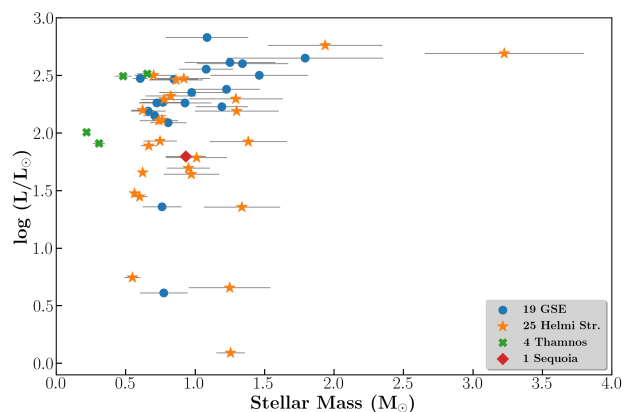


Fig. 7. Mass and luminosity of *HQ* candidate accreted stars identified through their orbit by Gaia Collaboration et al. (2023a). The considered accretion debris systems are indicated in the legend, together with the number of their member stars. The relative uncertainties in luminosity are equal to a few percent and are not visible in the logarithmic scale.

that are interpreted as signatures of past or ongoing merger events. Therefore, some stars belonging to the Galactic halo were formed in external galaxies in ancient epochs. Such merger debris stars can be identified through their specific Galactic orbits. For instance, they are located in specific regions in a diagram of the total energy (E) versus L_Z (vertical component of the angular momentum) (see, for instance, Fig. 25–27 in Gaia Collaboration et al. 2023a).

We adopted the list of candidate accreted *GSP-Spec* stars identified by Gaia Collaboration et al. (2023a). They belong to the *Gaia*-Enceladus-Sausage accreted galaxy (GES, Belokurov et al. 2018; Myeong et al. 2018; Helmi et al. 2018), the Sequoia (Myeong et al. 2019), the Thamnos (Koppelman et al. 2019; Helmi 2020), and the Helmi streams (Helmi et al. 1999). We cross-matched this list with the *HQ* subsample defined above, including the restriction $\log(g)_{\text{err}} < 0.1$ dex in order to select the most accurate derived masses. We show in Fig. 7 the stellar masses of the accretion debris candidate stars versus their luminosity. Most of these stars are high-luminosity stars with masses close to or lower than about $1 M_{\odot}$ (considering the uncertainties). These masses are fully consistent with the asteroseismic masses of GES stars derived by Montalbán et al. (2021). We also confirmed that these stars are all cool giants that left the main sequence a long time ago. The stellar masses of red giants are indeed a good proxy for their age, and typical ages for such post-main-sequence low-mass stars are older than ~ 10 – 12 Gy. This is fully compatible with the accretion epochs of the considered mergers. It is indeed thought that the GSE accretion occurred about 10 billion years ago (Helmi et al. 2018), about 5–8 Gyr ago for the Helmi stream (Koppelman et al. 2019), and between 8–11 Gyr ago for Sequoia; Thamnos is probably older (Dodd et al. 2025).

There are a few stars in Fig 7 that belong to GES or the Helmi stream, however, that are more massive than $\sim 1.5 M_{\odot}$ (therefore younger than the other candidates) or too faint to be giants. As already pointed out by Gaia Collaboration et al. (2023a), their sample of accreted stars belonging to the Helmi stream or GES is contaminated by disc stars because these streams lie close to the Galactic disc in the $E - L_Z$ plane. We therefore confirmed this contamination when we examined the stellar masses and/or luminosities. Based on these derived quantities, the contamination is stronger for the Helmi stream (it might reach up to $\sim 20\%$) than for GSE, which is closer to $\sim 10\%$. We thus emphasize that a

selection of merger debris stars based on purely kinematical criteria should be complemented by an examination of their chemical content (see, for instance, Fig 29 of Gaia Collaboration et al. 2023a), but also their mass (as proposed here) and/or age.

8. Summary

We have presented a new catalogue of interstellar colour excesses and extinctions, together with stellar luminosities, radii and masses for about 4.6 million stars. These data were computed from the *Gaia/GSP-Spec* atmospheric parameters (T_{eff} , $\log(g)$, $[M/H]$, and $[\alpha/Fe]$), derived from the analysis of the RVS spectra, combined with *Gaia/DR3* astrometry and photometry. These parameters are therefore fully compatible and homogeneous with the *Gaia/DR3* spectroscopic data. This procedure allowed us to avoid systematics and biases that might be hidden when data from different (and potentially) heterogeneous catalogues are combined. The uncertainties associated with all these new parameters were estimated based on 1,000 Monte-Carlo simulations for each star. We also included three quality flags in this catalogue that should be considered, together with the associated uncertainties, to define high-quality parameter subsamples. An example of such a *HQ* subsample, containing 1.5 million stars, is provided.

The high quality of the catalogue for dwarfs and giants (even when they are highly extinguished by the interstellar medium), was confirmed through different validations based on published interstellar maps, interferometric radii, and asteroseismic radii and masses. We found that the radius determinations have a similar precision as interferometric and asteroseismic determinations when similar effective temperatures were considered by us and the asteroseismic works. The relative mean differences between our mass determinations and the Kepler determinations are as small as a few percent, associated with a dispersion of 10-20%, when the agreement in surface gravity is good. This new catalogue, its large statistics, homogeneity, and high quality allowed us to explore different astrophysical problematics. Some example applications were described from exoplanets (de Laverny et al. 2025) to properties of the Galactic halo. For instance, we found that (i) the Present-Day Mass Function of the brightest giant stars is compatible with the Kroupa IMF when any metallicities are considered because of the different evolutionary timescales of low- and high-mass stars found in the different Galactic populations, (ii) the main Galactic populations can be identified directly based on their mass distribution, and (iii) the estimated low masses for the accreted halo stars are compatible with the epoch of their accretion into the Milky Way.

We finally emphasise that part of the methods we presented were adopted to calibrate the *Gaia/DR4 GSP-Spec* data that will be published in December 2026 (Palicio et al., in preparation). Moreover, a new version of this catalogue will be published after the *Gaia/DR4*, based on the new atmospheric parameter values derived from the RVS spectra. Its precision will be improved by the new implementations in the *GSP-Spec* pipeline. Improvements in the parameter accuracy are also expected because the uncertainties associated with the DR4 stellar parameters are lower since the S/N of the RVS spectra increases from DR3 to DR4. This catalogue size will also be extended by about a factor of 5-6 (i.e. a few tens of million stars) because more spectra are parametrised by *GSP-Spec* for the fourth *Gaia* data release.

Acknowledgements. This work has made use of data from the European Space Agency (ESA) mission *Gaia* (<https://www.cosmos.esa.int/gaia>), processed by the *Gaia* Data Processing and Analysis Consortium (DPAC,

<https://www.cosmos.esa.int/web/gaia/dpac/consortium>). Funding for the DPAC has been provided by national institutions, in particular the institutions participating in the Gaia Multilateral Agreement.

We acknowledge funding from the European Union's Horizon 2020 research and innovation program under SPACE-H2020 grant agreement number 101004214 (EXPLORE project).

This work has made use of the IPython package (Pérez & Granger 2007), NumPy (Harris et al. 2020), Matplotlib (Hunter 2007), Pandas, TOPCAT (Taylor 2005) and the SIMBAD database, operated at CDS, Strasbourg, France (Wenger et al. 2000). We also thank L. Casagrande for helpful discussions and the anonymous referee for his sensible comments. E.S thanks I.N.A.F. for the 1.05.24.07.02 Mini Grant – LEGARE “Linking the chemical Evolution of Galactic discs Across diverse scales: from the thin disc to the nuclear stellar disc” (PI E. Spitoni)

References

- Abdurro'uf, Accetta, K., Aerts, C., et al. 2022, *ApJS*, 259, 35
 Bailer-Jones, C. A. L., Rybizki, J., Fouvras, M., Demleitner, M., & Andrae, R. 2021, *AJ*, 161, 147
 Barbillion, M., Recio-Blanco, A., de Laverny, P., & Palicio, P. A. 2025, arXiv e-prints, arXiv:2511.12156
 Belokurov, V., Erkal, D., Evans, N. W., Koposov, S. E., & Deason, A. J. 2018, *MNRAS*, 478, 611
 Boltzmann, L. 1884, *Annalen der Physik*, 258, 291
 Borucki, W., Koch, D., Basri, G., et al. 2008, in *IAU Symposium*, Vol. 249, Exoplanets: Detection, Formation and Dynamics, ed. Y.-S. Sun, S. Ferraz-Mello, & J.-L. Zhou, 17–24
 Casagrande, L., Lin, J., Rains, A. D., et al. 2021, *MNRAS*, 507, 2684
 Casagrande, L., & Vandenberg, D. A. 2018, *MNRAS*, 479, L102
 Creevey, O. L., Sordo, R., Pailier, F., et al. 2023, *A&A*, 674, A26
 Cropper, M., Katz, D., Sartoretti, P., et al. 2018, *A&A*, 616, A5
 de Laverny, P., Ligi, R., Crida, A., Recio-Blanco, A., & Palicio, P. A. 2025, *A&A*, 699, A100
 de Laverny, P., Recio-Blanco, A., Aerts, C., & Palicio, P. A. 2024, *A&A*, 691, A182
 Dodd, E., Ruiz-Lara, T., Helmi, A., et al. 2025, *A&A*, 698, A277
 Duvert, G. 2016, *VizieR Online Data Catalog: JMDC : JMMC Measured Stellar Diameters Catalogue (Duvert, 2016)*, *VizieR On-line Data Catalog: II/345*. Originally published in: *JMMC center (2016)*
 Fulton, B. J., Petigura, E. A., Howard, A. W., et al. 2017, *AJ*, 154, 109
 Gaia Collaboration, Recio-Blanco, A., Kordopatis, G., et al. 2023a, *A&A*, 674, A38
 Gaia Collaboration, Vallenari, A., Brown, A. G. A., et al. 2023b, *A&A*, 674, A1
 Harris, C. R., Millman, K. J., van der Walt, S. J., et al. 2020, *Nature*, 585, 357
 Hayden, M. R., Recio-Blanco, A., de Laverny, P., et al. 2018, *A&A*, 609, A79
 Helmi, A. 2020, *ARA&A*, 58, 205
 Helmi, A., Babusiaux, C., Koppelman, H. H., et al. 2018, *Nature*, 563, 85
 Helmi, A., White, S. D. M., de Zeeuw, P. T., & Zhao, H. 1999, *Nature*, 402, 53
 Hunter, J. D. 2007, *Computing In Science & Engineering*, 9, 90
 Koppelman, H. H., Helmi, A., Massari, D., Price-Whelan, A. M., & Starkenburg, T. K. 2019, *A&A*, 631, L9
 Kroupa, P. 2002, *Science*, 295, 82
 Miglio, A., Chiappini, C., Morel, T., et al. 2013, *MNRAS*, 429, 423
 Montalbán, J., Mackereth, J. T., Miglio, A., et al. 2021, *Nature Astronomy*, 5, 640
 Myeong, G. C., Evans, N. W., Belokurov, V., Sanders, J. L., & Koposov, S. E. 2018, *MNRAS*, 478, 5449
 Myeong, G. C., Vasiliev, E., Iorio, G., Evans, N. W., & Belokurov, V. 2019, *MNRAS*, 488, 1235
 Navarrete, C., Recio-Blanco, A., de Laverny, P., & Escorza, A. 2025, *A&A*, 696, A82
 Palicio, P. A., Recio-Blanco, A., Poggio, E., et al. 2023, *A&A*, 670, L7
 Pérez, F. & Granger, B. E. 2007, *Computing in Science and Engineering*, 9, 21
 Pinsonneault, M. H., Elsworth, Y. P., Tayar, J., et al. 2018, *ApJS*, 239, 32
 Pinsonneault, M. H., Zinn, J. C., Tayar, J., et al. 2025, *ApJS*, 276, 69
 Prša, A., Harmanec, P., Torres, G., et al. 2016, *AJ*, 152, 41
 Recio-Blanco, A., de Laverny, P., Palicio, P. A., et al. 2024, *A&A*, 692, A235
 Recio-Blanco, A., de Laverny, P., Palicio, P. A., et al. 2023, *A&A*, 674, A29
 Rybizki, J., Green, G. M., Rix, H.-W., et al. 2022, *MNRAS*, 510, 2597
 Salaris, M., Chieffi, A., & Straniero, O. 1993, *ApJ*, 414, 580
 Salsi, A., Nardetto, N., Mourard, D., et al. 2020, *A&A*, 640, A2
 Scalo, J. M. 1986, *Fund. Cosmic Phys.*, 11, 1
 Schonhut-Stasik, J., Zinn, J. C., Stassun, K. G., et al. 2024, *AJ*, 167, 50
 Serenelli, A., Johnson, J., Huber, D., et al. 2017, *ApJS*, 233, 23
 Stefan, J. 1879, *Sitzungsber. Kaiserl. Akad. Wiss. Math. Naturwiss. Cl. II. Abth.*, 79, 391
 Taniguchi, D., de Laverny, P., Recio-Blanco, A., Tsujimoto, T., & Palicio, P. A. 2026, *A&A*, 707, A260
 Taylor, M. B. 2005, in *Astronomical Society of the Pacific Conference Series*, Vol. 347, *Astronomical Data Analysis Software and Systems XIV*, ed. P. Shopbell, M. Britton, & R. Ebert, 29
 Valle, G., Dell'Omodarme, M., Prada Moroni, P. G., & Degl'Innocenti, S. 2024, *A&A*, 690, A327
 Wenger, M., Ochsenbein, F., Egret, D., et al. 2000, *A&AS*, 143, 9
 Zinn, J. C., Stello, D., Elsworth, Y., et al. 2022, *ApJ*, 926, 191